Solid Freeform Fabrication 2017: Proceedings of the 28th Annual International Solid Freeform Fabrication Symposium – An Additive Manufacturing Conference
Reviewed Paper

Mesoscopic Multilayer Simulation of Selective Laser Melting Process

Subin Shrestha and Kevin Chou

Additive Manufacturing Research Center
University of Louisville
Louisville, KY 40292

Abstract

Selective Laser Melting (SLM) is a metal additive manufacturing with complex process physics that requires understanding of metallic particle accumulations and interactions to layer additions. In this work, a mesoscopic multilayer numerical model with volume of fluid (VOF) method is developed using ANSYS/FLUENT. At first, a sequential powder adding algorithm is applied to generate a layer of randomly distributed particles of non-uniform sizes over a solid substrate. A moving volumetric heat source is then applied to melt a single track in the powder layer which is defined by specifying temperature dependent material properties. After the single scan in the first layer is completed, the surface data is acquired to re-apply sequential powder adding algorithm over the deformed surface to generate second layer of powder. In this study, the melt flow has been simplified and is driven primarily by constant surface tension applied over the melt pool. The obtained track width from simulations is in reasonable agreement with experimental results in literature.

Keywords: Powder distribution; Selective laser melting; Thermo-fluid model.

1. Introduction

Selective Laser Melting (SLM) is an additive manufacturing (AM) process in which parts are built in a layer by layer fashion. At first, the powder particles are spread over build plate according to pre-defined layer thickness, which is then following by high speed laser scanning which results in rapid melting and solidification. Then, the second layer of powder is added over the first layer. This sequential addition and melting process continues until the desired part is produced. SLM process is associated with numerous process parameters such as laser power, scanning speed, layer thickness, scanning strategy, hatch spacing etc. The variation in each process parameter will affect the printed part and therefore each parameter needs careful consideration.

As the powder particles are melted, thermo-capillary effect comes into play which primarily governs the melt flow and its magnitude depends on process parameters being used. Besides, if the energy density is high enough to vaporize the metal, the recoil pressure acts upon the free surface which leads to the development of huge depression and possibly lead to formation of pores [1]. It has been shown that the geometry of the scan tracks depend on the process parameter used [2]. For high energy density, the heat penetration depth is very high, however for optimum energy density, there is no keyhole formation and the tracks formed by scanning is smooth. It is always desired to obtain the optimum process window for any material so as to establish quality control.

The entire SLM process can be broken down into layer by layer and each layer into scan line by scan line. The entire layers comprise of numerous scan lines whose orientation forms different scanning strategies. Study of formation of each scan track will help obtain the optimum process window for any material. There have been numerous experimental studies which focused on formation of single tracks for different materials. Yadroitsev et al. [3] experimentally studied the formation of single tracks for stainless steel (SS) grade 904L, SS grade 316L and CuNi10. The results indicated that the SLM process has a threshold character which separates instability zone where the scanning tracks are discontinuous and stability zone where the scanning tracks are continuous. Similarly, Li et al. [4] studied the balling characteristics of single scan tracks under different scanning speeds, laser powers and layer thickness. The balling formation generally occurs due to worsened wettability which becomes more significant as the layer thickness increases. The effect of scanning speed and laser power on track width and penetration depth has been studied for Inconel 625 [2]. The process parameters with low and high energy densities both produced porosities. Low energy density would lead to partial melting leading to formation of pores whereas at high energy density, the keyhole effect plays crucial role in formation of pores. Besides experimental study, various numerical studies have been performed so as to understand the fluid flow behavior which leads to formation single tracks. Khairallah and Anderson [5] developed a powder scale model which was able to predict the single tracks formation and the simulated track widths were in good agreement with the experiment. The initial model was simplified using constant surface tension which was enough to predict the surface formation. However, surface tension is a function of temperature and it should be incorporated in the model along with vaporization effect to accurately predict the fluid flow. Khairallah et al. [6] later developed a comprehensive model which was able to predict formation of depression, spatter, denudation area etc.

The single track experiments have been used to obtain the optimum process window for the combination of scanning speed and power. But a single layer has multiple tracks and therefore the spacing between these tracks also plays crucial role. Yadroitsev and Sumrov [7] noted that the changing of hatch spacing would lead to modification in the geometric characteristics of scan tracks as well as to the surface morphology. With the optimum combinations of scanning speed, laser power and hatch spacing a better surface morphology can be obtained. But, surface alone is not enough to establish SLM process; it is important to maximize the density. Su and Yang [8] studied the effect of hatch spacing on the inter-layer overlapping regime and concluded that hatch spacing lower than 0.2mm will produce high relative density parts. In addition, Lee and Zhang [9] developed a 3D thermo-fluid model using commercial Flow-3D software and back and forth scanning was used to predict the melt flow behavior and formation of tracks. The simulation result obtained after two-track scanning was compared with experiment and the model was able to predict the melt overlap and the depth. The surface roughness of a built layer will affect the formation of melt pool in the subsequent layer, which may lead to formation of interlayer pores and therefore undermine the strength of part. Moreover, the increasing the scanning speed would change the morphology of pores from near-spherical to elongated shape [10]. Such pores are undesirable and should be minimized. However, this requires great deal of experimentation and also poses a great challenge to understand the reason being formation of such pores. Therefore, numerical simulation may be applied to study of mechanism of formation of interlayer pores.

In this preliminary study, a 3D powder scale VOF model was developed to predict the single track formation during SLM process with random and uniform powder distributions. A moving-volumetric Gaussian heat source is applied to randomly distributed powder over solid substrate. The applied heat source immediately melts the powder and the solidified track is formed at the wake of beam. The single track formed is compared with experiment and thus formed free surface information is extracted and utilized to generate another layer of powder particles. Then, the second layer of powder particles are melted using same heat source. This process can be continued for multiple layers of simulation.

2. Methodology

2.1. Overall Methods

A powder scale model has been developed using ANSYS/FLUENT. In order to accurately capture fluid dynamics at the interface, VOF method has been applied. The powder particles with uniform and random distribution were generated by applying a sequential addition algorithm [11] with porosity of 55%. The powder particle information is read through User Defined Function (UDF) and the volumetric heat source is applied by continuously tracking the deforming surface. First scan track is obtained after completion of first layer scanning. After the completion, free surface data is extracted which is utilized as reference to generate second layer powder particles. After the powder particles have been generated, the second layer is scanned. Finally, different analyses are performed through post processing.

2.2. Thermal-fluid model and simulation

Model configuration:

3D thermo-fluid models were developed using ANSYS Fluent software. Figure 1 shows the overall domain of the model. The Inconel 625 powder particles are spread over 70 μm solid Inconel 625. Since the model domain is very small and there is no heat transfer through the walls due to adiabatic boundary conditions at faces, it would lead to residual temperature which balances throughout the domain during cooling period. Therefore, in order to reduce such effect a solid domain is added surrounding the powder particles which act as heat sink during cooling. The powder particles are distributed within 1600 μm and 450 μm plane as shown in the figure which is surrounded by 200 μm solid Inconel in each side. Fine mesh of 5 μm is applied at the powder and interface region. All the elements in the model are hexahedron type for better prediction of interface with VOF method. The blue zone is the argon gas where there is no volume fraction of In625, and therefore the phase-2 volume fraction in this region is 0. The red zone represents both solid base and powder as this is a two phase simulation. And the free surface of the powder lies between volume fraction of 0 and 1. The solid base is designed such that it is bigger than the melt pool depth such that the boundary does not interfere with the melt flow. The scan length of 1.2 mm is used for all simulation.

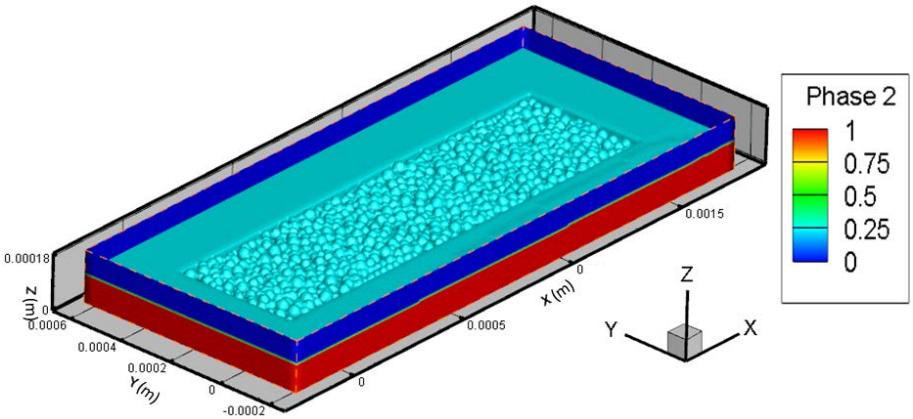

Figure 1: 3D powder scale model thermo-fluid simulation.

Governing equations:

The laser heat source has been modeled as a moving Gaussian distribution heat source in horizontal direction with a linear decaying in vertical direction. Therefore, the conical volumetric heat source was represented as Eqn (1) below:

$$\dot{Q}_{(x,y,z)} = \eta \times \frac{H_S \times I_Z}{S} \qquad (1)$$

Where,

$$I_z = \frac{1}{0.75}\left(-2.25\left(\frac{z}{S}\right)^2 + 1.5\left(\frac{z}{S}\right) + 0.75\right),$$

$$H_s = \frac{2P}{\pi d^2}\exp\left\{-\frac{2\left[(x-x_s)^2+(y-y_s)^2\right]}{d^2}\right\}.$$

in which the parameters include laser beam absorption efficiency coefficient: η, power: P, optical penetration depth: S, beam diameter: d, x_S and y_S: heat source center position. Hs and I_z are horizontal Gaussian distribution heat source and heat source magnitude decaying function in vertical direction, respectively. The heat source is defined in the UDF and applied as the source term in energy equation.

Tracking of free surface

The basic governing equations associated with the Thermo-fluid model have been presented [12]. In this study, VOF model is used to track the free surface. The VOF function is defined to indicate the topology of metal flow. The VOF equation is given as

$$\frac{\partial F}{\partial t} + \vec{v}.\nabla F = 0 \qquad (2)$$

Where, F represents the volume fraction and $\vec{v}$ represents the velocity vector. In this model, two phases have been used-argon and Inconel 625. A free surface of the powder which interacts with the argon has the volume fraction between 0 and 1. UDF is used to identify the free surface mesh to appropriately apply the volumetric heat source.

Boundary conditions

The boundary condition at the interface is given as

$$\frac{\partial(\rho H)}{\partial t} + \frac{\partial(\rho u_i H)}{\partial x_i} = \frac{\partial}{\partial x_i}\left(k\frac{\partial T}{\partial x_i}\right) + \dot{Q}(x,y,z) - hA(T - T_\infty) - \sigma A\varepsilon(T^4 - T_\infty^4) \qquad (3)$$

Where, H is the enthalpy, k is thermal conductivity, $\dot{Q}_{(x,y,z)int}$ is the heat source applied at the interface, h is the heat transfer coefficient, σ is the Stefan-Boltzmann constant and ε is the

emissivity which is used to account for the radiation through the top surface and A is the free surface area of cell. Besides, all the faces in the domain have adiabatic boundary conditions.

Application of volumetric heat source

The free surface in powder scale model is not flat and therefore it needs to be properly identified in order to apply volumetric heat source. In addition, the surface is continuously deforming during the melting process. Therefore, the topmost cell with non-zero phase-2 (In625) volume fraction which is the actual free surface has to be tracked after iteration and is achieved by storing cell information to user defined cell variable in UDF. The free surface cell information is stored and utilized to define the magnitude of heat source for other cells.

Material Properties

The physical properties such as thermal conductivity, specific heat, density are the function of temperature. Therefore, the temperature dependent material properties summarized in figure 2 are used to define solid and powder Inconel 625. As the properties are almost linear with the temperature, they are defined as piece-wise linear in Fluent. Besides these, surface tension is also the function of temperature. Additional material properties of Inconel 625 have been summarized in table 1. Generally the surface tension of metal can be defined by the equation 1.

$$\gamma = \gamma_m + \frac{d\gamma}{dT}\Delta T \qquad (4)$$

Where γ is the surface tension, γ_m is the surface tension at the melting point, $\frac{d\gamma}{dT}$ is the surface tension gradient and ΔT is the temperature difference. In this study, only constant surface tension has been considered. Moreover, the surface tension for Inconel 625 has been approximated with that of Inconel 718 [9].

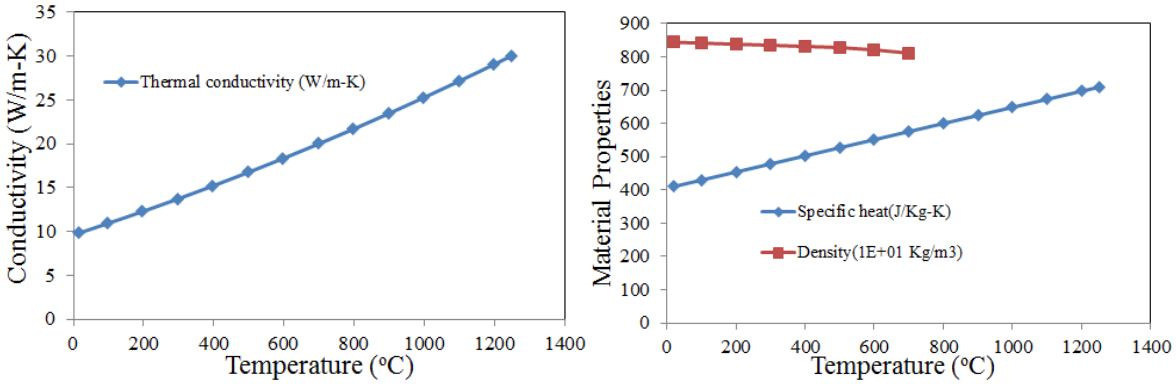

Figure 2: Temperature dependent material properties of solid Inconel 625 [13].

Table 1: Properties of Inconel 625

Parameters	Values
Solidus temperature, T_S (°C)	1290
Liquidus temperature, T_L (°C)	1350 [14]
Latent heat of fusion, L_f (kJ/Kg)	227
Power (W)	195

Scanning speed (mm/s)	800
Layer thickness (μm)	30
Viscosity(kg/m-s)	0.006
Emissivity, ε	0.5 [15]
Stefan-Boltzmann constant, σ	5.67×10^{-8}

2.3. First layer simulation

The sequential drop down algorithm is used to generate first layer of powder particles. Normal distribution with the range of 20-40 μm and uniform distribution with powder diameter 30 μm are generated using a developed program. A section cut along scanning direction and transverse direction of the powder distributed over substrate has been presented in figure 3. As seen in the figure, there is huge contact between powder and solid, which is due to the mesh size. This may slightly under-predict the temperature response due to better heat transfer at the contact region. The volumetric heat source is applied with reference of free surface of each powder particles. As the scanning continues, the powder particles are continuously melted when laser interacts with powder, whereas the melt pool beings to solidify at the wake of the beam. The fluid flow within the melt pool results in formation of single tracks with certain width and height. The formed track may depend on the distribution of the powder particles.

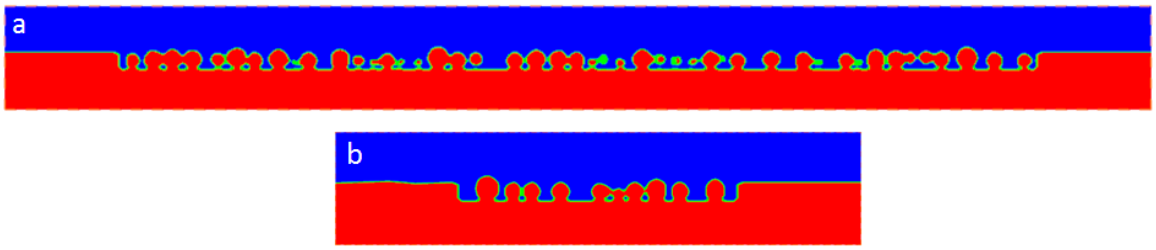

Figure 3: (a) Normal powder distribution in scanning direction and (b) transverse direction in a first layer

2.4. Second layer simulation

As the first layer simulation is completed, the single track is let to solidify considering the recoating time. The free surface after solidification is obtained from fluent post processor and mesh information is extracted. The mesh information contains all the details of the free surface, but only the co-ordinate information is required for reference. The mesh co-ordinate information is utilized as the reference for base for second layer powder addition algorithm. The algorithm for second layer powder addition, which is a modification of first layer powder addition, is used and the powder particles are distributed over the first layer surface. Due to huge number of mesh at the free surface, the second layer powder generation takes significantly longer time compared to first layer which is distributed over flat plate. The cross section of the normal distribution of the powder particles is shown in figure 4. We may observe the surface from first layer is not flat which would affect the powder particle distribution. Once the powder is defined, the volumetric source is used to melt the second layer of powder particles. At the current stage, the stability of

powder particles when dropping over previous layer has not been fully defined due to difficulty in identifying the curvature of the free surface. The algorithm does not account for the force exerted by one particle on another, but would still be reasonable to model the normal distribution of powder particles.

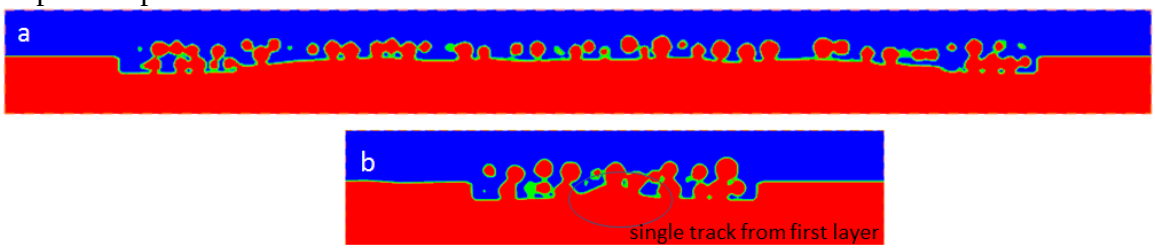

Figure 4: (a) Powder distribution in scanning direction and (b) transverse direction in second layer

3. Results and Discussion

3.1. First layer simulation results

The temperature profile during the melting has been shown in figure 5(a). During the melting, temperature reaches around 2799 K which ensures proper melting but is below evaporation temperature. Thus, there would be no keyhole feature in this case. As the laser beam moves, the melt pool continues to solidify at the tail region. The continuous melting, fluid flow within melt pool and rapid solidification lead to such deformed surface. Figure 5(b) compares the top view of single track result predicted by simulation with the experimental result. With 195 W power and 800 mm/s scanning speed, the energy density is optimum which resulted in smooth and dense track and the simulation result is in good agreement with the experiment. Furthermore, the track width of the simulation is compared to the experiment for detailed comparison. Only one section is available from the experimental result. However, the track width would depend on the position of the cut. Therefore, no statistical comparison has been made at this time. The track width, in general, for simulation result is around 122 ± 7 μm which is very close to 128 μm obtained from experiment for a specific cross section. After the first layer scanning is completed, the heat source is turned off considering the recoating time. However, due to very small domain size, the temperature balances after 1 second of simulation time. The added heat sink would minimize the residual heat but was not enough to drop it to reasonable amount and the temperature of the all domain balances to 473 K. This issue may be resolved by enlarging the surrounding solid domain or changing addition heat transfer boundary condition against adiabatic boundary condition.

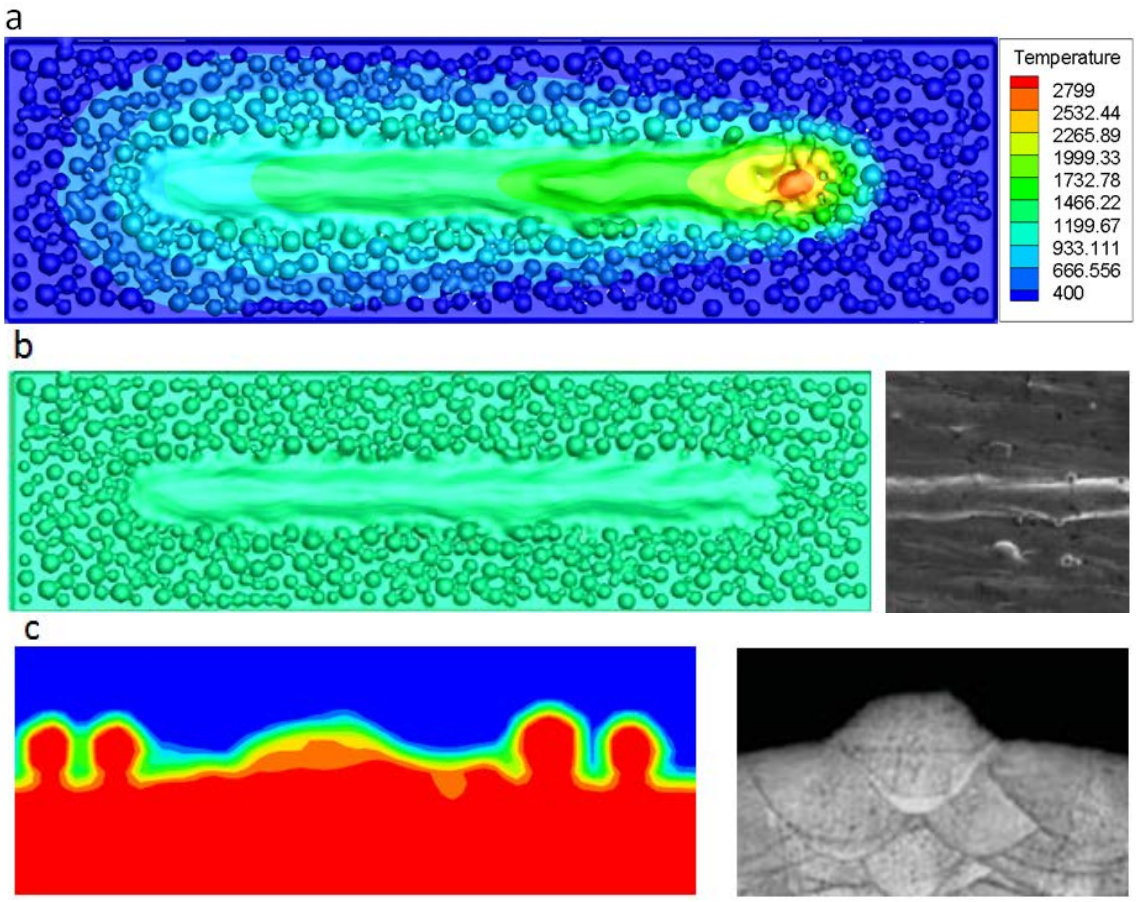

Figure 5: (a) Temperature distribution during first layer scanning, (b) simulation result compared with the experiment single track [2] and (c) transverse section comparison between simulation and experiment.

The surface formation may depend on the powder distribution. Therefore, another simulation is performed with uniform powder distribution to study its effect on the surface formation. The temperature distribution is shown in figure 6 (a). Temperature at an instant in powder scale model depends on the powder density at the beam center. At this instant the maximum temperature is 2620 K which is lower than that from normal powder distribution. This may be due to higher gap between powder particles at uniform distribution at that location. The single track morphology has been depicted in figure 6(b). But, it is difficult to compare the result between normal distribution and uniform distribution as the single tracks look similar. The transverse track geometry is the function of location as shown in figure 6(c) and the track width will also vary along the scanning direction. The track width is smaller compared to random powder distribution, primarily due to lower melt pool size for uniform distribution. All of this relates to the temperature prediction, when temperature is higher, the melt pool gets bigger, and eventually the track width is affected.

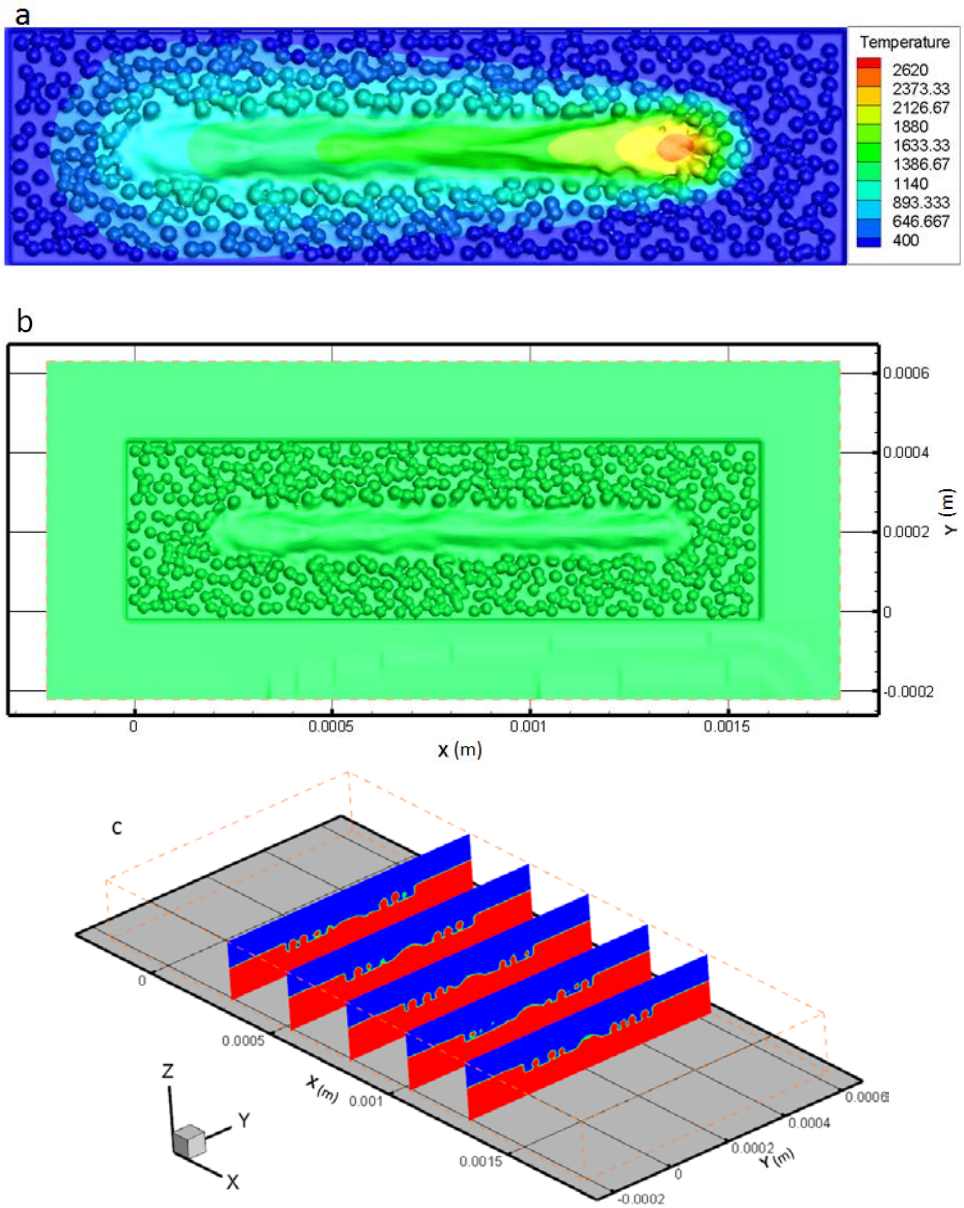

Figure 6: (a) Temperature distribution during first layer scanning with uniform 30 µm powder distribution, (b) Single track morphology and (c) Transverse shape at different locations.

3.2. Second layer simulation results

After the first layer scanning is completed, powder particles are distributed over first layer and again scanned with volumetric heat source. Figure 7(a) shows the solidified scan track; the temperature 1350 K is below the melting point of In625. Figure 7(b) shows the transverse section of the scan track. There is no significant change in width compared to first track. Moreover, the volume fraction of the solidified track shows that the scanned area is dense. The optimum process parameter has been used which forms high density tracks. If lower energy density had been used, we may have observed lower density regions at the interface or even pores. The developed model will be utilized in future to study process parameter effect on variation in density during multi-layer scanning. Also, it is important to note that due to limited

domain size and adiabatic boundary conditions at walls, the residual temperature from first layer scanning will highly affect the second layer melting process. Therefore, a more suitable boundary condition has to be applied so that the model size may not be increased as this would incur additional computational time.

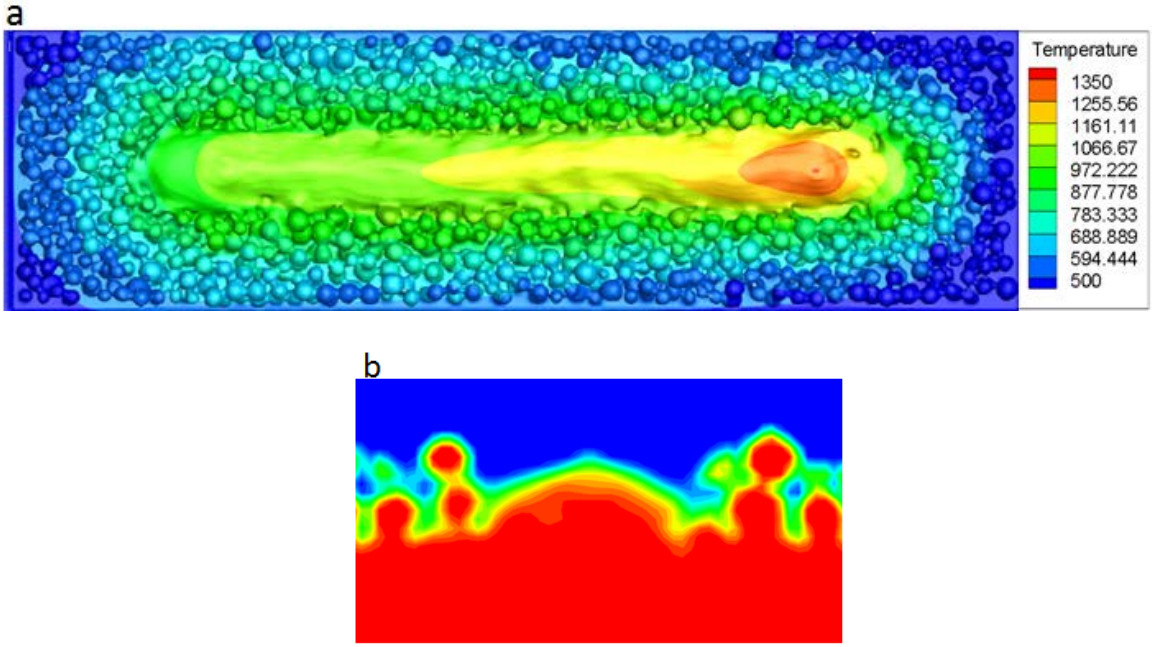

Figure 7: (a) Single track morphology after second layer simulation with normal powder distribution and (b) transverse section of single track.

The solidified track of second layer simulation for uniform powder distribution has been shown in figure 8 (a). It looks that the powder distribution will have minimal effect when optimum process parameter is used. Although it is difficult to make concrete conclusions from the single track, we may say that the powder distribution would have minimum effect on build surface roughness as the track width has very little difference. Figure 8(b) shows the track cross section at 5 different locations.

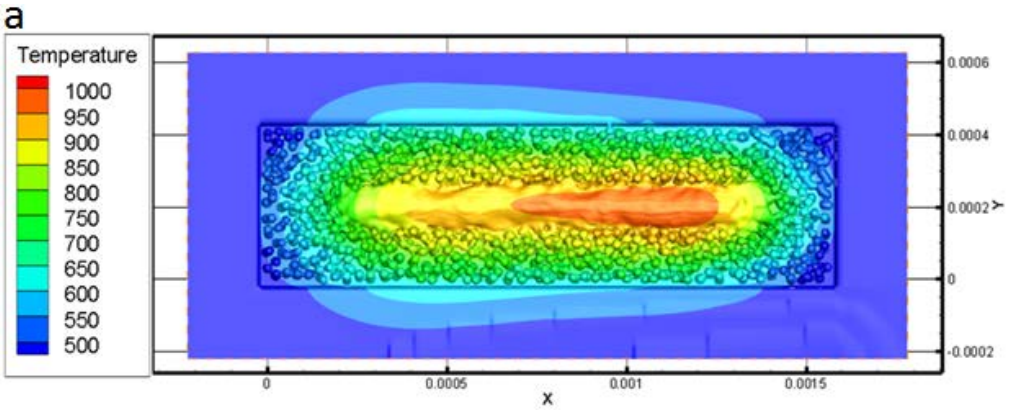

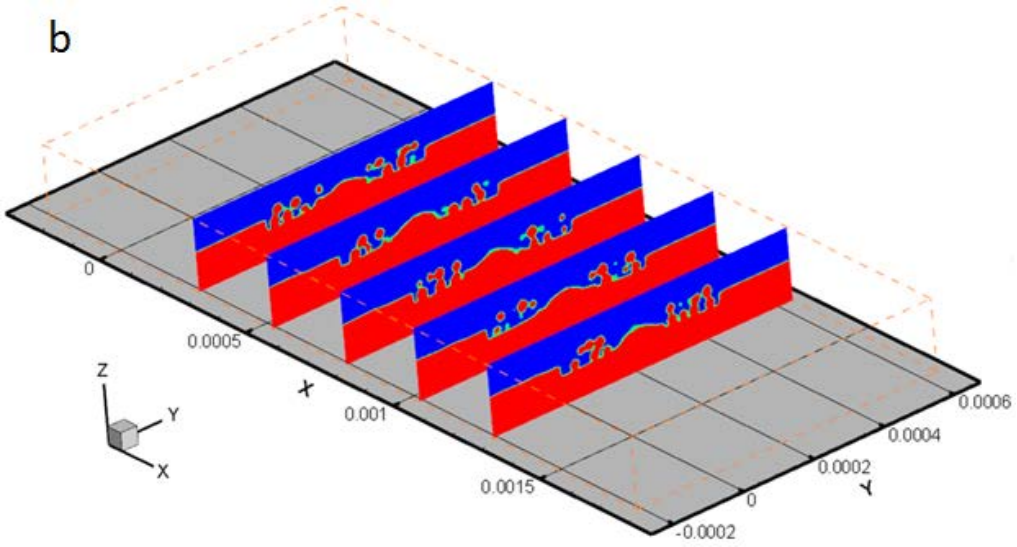

Figure 8: (a) Single track morphology formed with uniform 30 μm powder distribution in second layer and (b) corresponding transverse shape at different locations.

4. Conclusions

In this study, a sequential powder adding algorithm has been applied to generate randomly and normally distributed powder particles. The powder particles are heated by a laser source and the VOF model was employed using ANSYS/FLUENT software so as to study the free surface formation during melting and subsequent solidification. In addition, a multilayer simulation is proposed and following conclusions can be drawn from the simulation results.

- Powder-scale model can be applied to predict the formation of single tracks which would help to optimal process parameters. The single track predicted by simulations was in reasonable agreement with experimental results from literature.
- Powder particles can be added to a free surface obtained from the previous layer processing to perform second layer scanning. The formation of interlayer pores may be revealed by such a study.
- The thermal response depends on the powder distribution; in general, the melt pool size increases when the powder particle density exposed to laser increases.

Acknowledgement

This research is partially supported by NIST (70NANB16H029) and NSF (1662662).

References

[1] Aboulkhair, N. T., Maskery, I., Tuck, C., Ashcroft, I., and Everitt, N. M., 2016, "On the formation of AlSi10Mg single tracks and layers in selective laser melting: Microstructure and nano-mechanical properties," Journal of Materials Processing Technology, 230, pp. 88-98.

[2] Dilip, J., Anam, M. A., Pal, D., and Stucker, B., "A short study on the fabrication of single track deposits in SLM and characterization."
[3] Yadroitsev, I., Gusarov, A., Yadroitsava, I., and Smurov, I., 2010, "Single track formation in selective laser melting of metal powders," Journal of Materials Processing Technology, 210(12), pp. 1624-1631.
[4] Li, R., Liu, J., Shi, Y., Wang, L., and Jiang, W., 2012, "Balling behavior of stainless steel and nickel powder during selective laser melting process," The International Journal of Advanced Manufacturing Technology, 59(9-12), pp. 1025-1035.
[5] Khairallah, S. A., and Anderson, A., 2014, "Mesoscopic simulation model of selective laser melting of stainless steel powder," Journal of Materials Processing Technology, 214(11), pp. 2627-2636.
[6] Khairallah, S. A., Anderson, A. T., Rubenchik, A., and King, W. E., 2016, "Laser powder-bed fusion additive manufacturing: physics of complex melt flow and formation mechanisms of pores, spatter, and denudation zones," Acta Materialia, 108, pp. 36-45.
[7] Yadroitsev, I., and Smurov, I., 2011, "Surface morphology in selective laser melting of metal powders," Physics Procedia, 12, pp. 264-270.
[8] Su, X., and Yang, Y., 2012, "Research on track overlapping during selective laser melting of powders," Journal of Materials Processing Technology, 212(10), pp. 2074-2079.
[9] Lee, Y., and Zhang, W., 2016, "Modeling of heat transfer, fluid flow and solidification microstructure of nickel-base superalloy fabricated by laser powder bed fusion," Additive Manufacturing, 12, pp. 178-188.
[10] Panwisawas, C., Qiu, C., Sovani, Y., Brooks, J., Attallah, M., and Basoalto, H., 2015, "On the role of thermal fluid dynamics into the evolution of porosity during selective laser melting," Scripta Materialia, 105, pp. 14-17.
[11] Zhou, J., Zhang, Y., and Chen, J., 2009, "Numerical simulation of random packing of spherical particles for powder-based additive manufacturing," Journal of Manufacturing Science and Engineering, 131(3), p. 031004.
[12] Shrestha, S., and Chou, K., 2017, "A Build Surface Study of Powder-Bed Electron Beam Additive Manufacturing by 3D Thermo-fluid Simulation and White-light Interferometry," International Journal of Machine Tools and Manufacture.
[13] Capriccioli, A., and Frosi, P., 2009, "Multipurpose ANSYS FE procedure for welding processes simulation," Fusion Engineering and Design, 84(2), pp. 546-553.
[14] Lemster, K., Delporte, M., Graule, T., and Kuebler, J., 2007, "Activation of alumina foams for fabricating MMCs by pressureless infiltration," Ceramics international, 33(7), pp. 1179-1185.
[15] Kobayashi, M., Otsuki, M., Sakate, H., Sakuma, F., and Ono, A., 1999, "System for measuring the spectral distribution of normal emissivity of metals with direct current heating," International journal of thermophysics, 20(1), pp. 289-298.